

Unraveling the acoustic electron-phonon interaction in graphene

Kristen Kaasbjerg,* Kristian S. Thygesen, and Karsten W. Jacobsen
*Center for Atomic-scale Materials Design (CAMD),
Department of Physics, Technical University of Denmark*
(Dated: November 1, 2018)

Using a first-principles approach we calculate the acoustic electron-phonon couplings in graphene for the transverse (TA) and longitudinal (LA) acoustic phonons. Analytic forms of the coupling matrix elements valid in the long-wavelength limit are found to give an almost quantitative description of the first-principles based matrix elements even at shorter wavelengths. Using the analytic forms of the coupling matrix elements, we study the acoustic phonon-limited carrier mobility for temperatures 0 – 200 K and high carrier densities of $10^{12} - 10^{13} \text{ cm}^{-2}$. We find that the intrinsic *effective* acoustic deformation potential of graphene is $\Xi_{\text{eff}} = 6.8 \text{ eV}$ and that the temperature dependence of the mobility $\mu \sim T^{-\alpha}$ increases beyond an $\alpha = 4$ dependence even in the absence of screening when the full coupling matrix elements are considered. The large disagreement between our calculated deformation potential and those extracted from experimental measurements (18 – 29 eV) indicates that additional or modified acoustic phonon-scattering mechanisms are at play in experimental situations.

PACS numbers: 81.05.Hd, 72.10.-d, 72.20.-i, 72.80.Jc

I. INTRODUCTION

Since the experimental realization of graphene,¹ its electronic properties and their understanding have been studied extensively both experimentally and theoretically.²⁻⁴ While the intrinsic carrier mobility of graphene is predicted to be exceptionally high, the experimental reality in substrate supported graphene involving charged impurities, electron-hole puddles, surface-optical phonons of the substrate, and disorder typically results in strongly reduced mobilities compared to the expected intrinsic value.^{5,6} Together with scattering on acoustic phonons which manifests itself in a linear temperature dependence of the mobility at higher temperatures, these extrinsic scattering mechanisms typically dominate the mobility. The linear temperature dependence characteristic for acoustic phonon scattering has so far been observed in both supported^{5,7-10} and suspended¹¹ graphene samples.

With the recent improvements in sample fabrication, the relative role of acoustic phonon scattering must be expected to become increasingly important in future devices. For example, samples with the commonly used SiO_2 substrate replaced by hexagonal boron nitride (h-BN) which has a lattice constant very close to that of graphene and an almost atomically flat surface with strongly reduced disorder,^{12,13} have shown highly improved transport characteristics with mobilities approaching that of suspended graphene.^{8,14,15} Furthermore, the high energy of the surface-optical phonons of h-BN results in a significant reduction of surface-optical phonon scattering¹⁶⁻¹⁸ that for commonly used gate oxides starts to dominate the mobility around $T \sim 150 - 200 \text{ K}$.^{5,9}

When the mobility is dominated by acoustic phonon scattering, two transport regimes separated by the Bloch-Grüneisen (BG) temperature $T_{\text{BG}} = 2\hbar k_F c_{\text{ph}}/k_B$ can

be identified.¹⁹ Here, k_F is the Fermi wave vector, c_{ph} the sound velocity and k_B the Boltzmann constant ($T_{\text{BG}} \sim 57 \text{ K} \sqrt{n}$ for the LA phonon with n measured in units of 10^{12} cm^{-2}). Since the BG temperature corresponds to the acoustic phonon energy $\hbar\omega_{\mathbf{q}} = \hbar c_{\text{ph}}q$ for full backscattering at the Fermi level, short wavelength acoustic phonons are frozen out at temperatures $T < T_{\text{BG}}$ restricting scattering processes to small scattering angles. The restricted phase space available for phonon scattering at $T < T_{\text{BG}}$ results in a transition from the linear $\rho \sim T$ behavior of the resistivity in the high-temperature regime to a stronger $\rho \sim T^\alpha$ temperature dependence in the BG regime where $\alpha = 4$ ($\alpha = 6$) in the absence (presence) of screening by the carriers themselves.^{20,21} The BG behavior in the temperature dependence of the mobility (resistivity) has recently been observed experimentally.⁷

Existing theoretical^{20,21} and experimental^{5,7-9,11} studies of acoustic phonon-limited transport in graphene often parametrize the interaction with acoustic phonons in terms of a coupling to a single *effective* acoustic phonon. The associated deformation potential coupling constant extracted from the experimentally measured temperature dependence of the resistivity range from $\sim 18 - 29 \text{ eV}$.^{5,7-9,11} On the other hand, theoretical studies of the acoustic electron-phonon coupling yield much lower values on the order of $3 - 4.5 \text{ eV}$.^{22,23} At the same time, different forms of the coupling matrix element are used in theoretical studies^{20,22} making a direct comparison of the different values of the deformation potential difficult.

Even though the effect of acoustic phonon scattering on the carrier mobility in graphene has been studied widely in the literature,^{20,23-27} a complete study considering the full details of the coupling matrix element is still lacking. The purpose of the present study is to provide a detailed analysis of the acoustic electron-phonon inter-

action in graphene and to establish the intrinsic value of the effective deformation potential. We shall focus on supported graphene where the flexural phonons are quenched and hence include only the transverse (TA) and longitudinal (LA) acoustic phonons. We use a first-principles method to calculate the electron-phonon interaction^{28,29} supported by the group-theoretical considerations of Ref.30. We then study the intrinsic phonon-limited mobility using a Boltzmann equation approach in the temperature regime 0 – 200 K and for high carrier densities $n \sim 10^{12} - 10^{13} \text{ cm}^{-2}$ where screening by the carriers suppresses other scattering mechanisms. Using the full coupling matrix elements, we find that a temperature dependence with $\alpha > 4$ occurs even in the absence of screening.

II. THEORY

In the following, the carriers in graphene are described by massless Dirac fermions with linear dispersion $\varepsilon_{\mathbf{k}} = \hbar v_F k$ where $v_F \sim 1.0 \times 10^6 \text{ m/s}$ is the Fermi velocity. Within the Boltzmann equation approach,^{6,25,31} the mobility in graphene in the presence of (quasi) elastic scattering mechanisms is given by

$$\mu_{xx} = \frac{\sigma_{xx}}{ne} = \frac{e v_F^2 \langle \tau_{\mathbf{k}} \rangle}{2} \quad (1)$$

where σ_{xx} is the conductivity, n is the two-dimensional carrier density and the density-of-states averaged relaxation time (in units of time per energy) is defined by

$$\langle \tau_{\mathbf{k}} \rangle = \frac{1}{n} \int d\varepsilon_{\mathbf{k}} \rho(\varepsilon_{\mathbf{k}}) \left(-\frac{\partial f}{\partial \varepsilon_{\mathbf{k}}} \right) \tau_{\mathbf{k}}. \quad (2)$$

Here, $\rho(\varepsilon_{\mathbf{k}}) = (g_s g_v / 2\pi \hbar^2) \varepsilon_{\mathbf{k}} / v_F^2$ is the density of states of the graphene layer and $g_s = 2$ and $g_v = 2$ are the spin and valley degeneracies, respectively. At low temperatures and high carrier densities where $\varepsilon_F \gg k_B T$ this yields $\mu_{xx} \approx e v_F^2 \tau_{k_F} / \varepsilon_F$.

In the case of acoustic phonon scattering which can be treated as a quasielastic process, the relaxation time for each of the acoustic phonons (TA and LA) is given by²⁰

$$\frac{1}{\tau_{\mathbf{k}\lambda}} = \sum_{\mathbf{k}'} (1 - \cos \theta_{\mathbf{k},\mathbf{k}'}) P_{\mathbf{k}\mathbf{k}'}^\lambda \frac{1 - f_{\mathbf{k}'}}{1 - f_{\mathbf{k}}}, \quad (3)$$

where $\theta_{\mathbf{k},\mathbf{k}'}$ is the scattering angle and $f_{\mathbf{k}} = f(\varepsilon_{\mathbf{k}})$ the Fermi function. The transition matrix element is given by

$$P_{\mathbf{k}\mathbf{k}'}^\lambda = \frac{2\pi}{\hbar} \sum_{\mathbf{q}} |g_{\mathbf{q}\lambda}|^2 \left[N_{\mathbf{q}\lambda} \delta(\varepsilon_{\mathbf{k}'} - \varepsilon_{\mathbf{k}} - \hbar\omega_{\mathbf{q}\lambda}) + (1 + N_{\mathbf{q}\lambda}) \delta(\varepsilon_{\mathbf{k}'} - \varepsilon_{\mathbf{k}} + \hbar\omega_{\mathbf{q}\lambda}) \right]. \quad (4)$$

Here, $g_{\mathbf{k}\mathbf{q}}^\lambda$ is the electron-phonon coupling, λ denotes the acoustic phonon branches, and $\hbar\omega_{\mathbf{q}\lambda}$ the acoustic

phonon energy. In the following, these quantities are calculated from first-principles. The phonons are assumed to be in equilibrium and populated according to the Bose-Einstein distribution function $N_{\mathbf{q}\lambda} = N(\hbar\omega_{\mathbf{q}\lambda})$. As scattering on both the TA and LA phonon is considered here, the total relaxation time for the K, K' -valleys is given by the sum of the individual phonon contributions as $\tau^{-1} = \sum_{\lambda} \tau_{\lambda}^{-1}$. As we show in the following section, the matrix elements of the electron-phonon coupling differ in the K and K' valleys (see e.g. Fig. 1). The Boltzmann equation must therefore be solved explicitly in both valleys. In the absence of intervalley scattering which couples the distribution functions in the two valleys, this can be done by considering the two valleys separately. In this case, the relaxation time entering the expression for the mobility in Eq. (1) becomes the valley-averaged relaxation time $\tau = (\tau_K + \tau_{K'})/2$, where $\tau_{K/K'}$ is the total relaxation time in the individual valleys. Screening of the electron-phonon interaction by the carriers themselves^{32,33} has been considered elsewhere²¹ and will here be neglected.

While analytic considerations have been given in Refs.20,21, we will in the present work resort to a numerical evaluation^{34,35} of the relaxation time in Eqs. (3) and (4). This allows us to study the acoustic phonon-limited mobility in graphene with the full coupling matrix elements which have a more complex angular dependence than most often assumed (see e.g. Ref.20). The numerical approach also allows for a unified treatment of the high-temperature ($T > T_{\text{BG}}$) and Bloch-Grüneisen ($T < T_{\text{BG}}$) regimes. We note, however, that in the low-temperature regime where $\hbar\omega_{\mathbf{q}} \sim k_B T$, it is crucial that the phonon energy is retained in the Fermi function in Eq. (3). In the high-temperature regime this requirement can be relaxed and the relaxation time can be put on a simple analytic form.

III. INTERACTION WITH ACOUSTIC PHONONS

In the following we use a first-principles DFT approach based on a fully microscopic description of both the electronic Bloch states and the phonons to calculate the acoustic electron-phonon couplings in graphene.^{28,29,36} The calculated values for the sound velocities c_λ for the TA and LA phonons are reported in Table I together with other parameters used in this work. Due to their high phonon energies ($> 100 \text{ meV}$), acoustic intervalley and optical phonons do not play a role in the considered temperature range and can therefore be neglected.

The interaction between charge carriers and the acoustic phonons in graphene can be written in the general form

$$g_{\mathbf{k}\mathbf{q}}^\lambda = \sqrt{\frac{\hbar}{2A\rho\omega_{\mathbf{q}\lambda}}} M_{\mathbf{k}\mathbf{q}}^\lambda, \quad (5)$$

where A is the area of the graphene layer, ρ is the mass

density and $M_{\mathbf{k}\mathbf{q}}^\lambda = \langle \mathbf{k} + \mathbf{q} | \delta V_{\mathbf{q}\lambda} | \mathbf{k} \rangle$ is the coupling matrix element for scattering between the two Bloch states \mathbf{k} and $\mathbf{k} + \mathbf{q}$ due to a phonon with wave vector \mathbf{q} , branch index λ and frequency $\omega_{\mathbf{q}\lambda} = c_\lambda q$ where c_λ is the sound velocity for the acoustic branches. The coupling is mediated by the change $\delta V_{\mathbf{q}\lambda}$ in the microscopic crystal potential due to a unit displacement of the atoms along the mass-scaled normal mode vector $\mathbf{e}_{\mathbf{q}\lambda}$. Due to the full microscopic treatment of both electrons and phonons, Umklapp processes involving reciprocal lattice vectors are included in the coupling matrix element $M_{\mathbf{k}\mathbf{q}}^\lambda$.

Figure 1 shows the absolute value of the coupling matrix elements $M_{\mathbf{k}\mathbf{q}}^\lambda$ to the TA and LA phonons in the K, K' valleys as a function of the two-dimensional phonon wave vector \mathbf{q} . The matrix elements in the two valleys are related through time-reversal symmetry as $M_{\mathbf{k}\mathbf{q}}^{K\lambda*} = M_{-\mathbf{k}, -\mathbf{q}}^{K'\lambda}$. This implies that carriers in the two valleys traveling in the same direction experience different electron-phonon couplings. It should be emphasized that the calculated matrix elements include the full symmetry of both the electronic Bloch states and the phonon modes as given by the complete microscopic description.

In order to emphasize the effect of the chirality of the carriers in graphene, the initial carrier state \mathbf{k} is located on the right side of the Dirac cones 300 meV above the K, K' -points as indicated by the sketch in the top of the figure. As is evident from the figure, both the TA and LA phonons couple to the carriers with similar coupling strengths. While backscattering is suppressed for the LA mode, the situation is reversed for the TA mode where forward scattering is suppressed. In addition to suppression of forward and backscattering, other directions with complete suppression of scattering also appears. This is a consequence of the inclusion of the symmetry of both phonons and electronic states.

Parameter	Symbol	Value
Lattice constant	a	2.46 Å (LDA)
Ion mass density	ρ	7.6×10^{-8} g/cm ²
Fermi velocity	v_F	1.0×10^6 m/s
Transverse sound velocity	c_{TA}	14.1×10^3 m/s
Longitudinal sound velocity	c_{LA}	21.2×10^3 m/s
Electron-phonon couplings		
Transverse	β_{TA}	2.8 eV
Longitudinal	α_{LA}	2.8 eV
Longitudinal	β_{LA}	2.5 eV
Effective coupling parameters		
Sound velocity	c_{eff}	20.0×10^3 m/s
Deformation potential	Ξ_{eff}	6.8 eV

TABLE I: Material parameters for graphene used in the present work. The phonon related parameters have been obtained from first-principles as described in the text. The calculated sound velocities are in excellent agreement with the values reported in Ref.27.

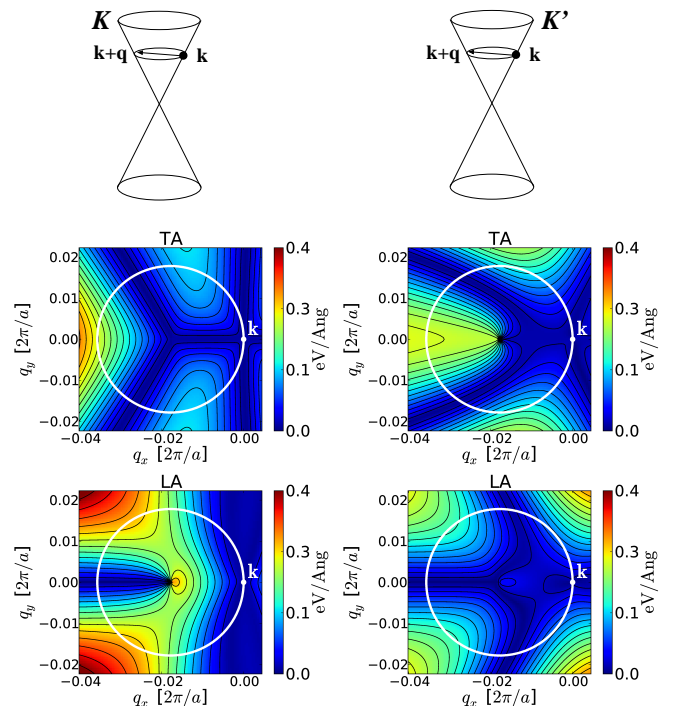


FIG. 1: (Color online) Electron-phonon couplings to the acoustic TA and LA phonons in the K, K' -valleys (left and right columns, respectively) of graphene. The contour plots show the absolute value of the coupling matrix elements $|M_{\mathbf{k}\mathbf{q}}^\lambda|$ for a carrier energy of 300 meV as a function of the two-dimensional phonon wave vector \mathbf{q} . The (white) circles correspond to $\mathbf{k} + \mathbf{q}$ vectors lying on the constant energy surfaces of the Dirac cones given by the energy $\epsilon_{\mathbf{k}}$ of the initial state in \mathbf{k} as sketched in the top row.

In the following, the first-principles coupling matrix elements are analyzed using the group-theoretical analysis of the electron-phonon interaction presented in Ref.30. In the long-wavelength limit, the TA and LA phonons are strictly transverse and longitudinal, respectively,³⁷ and the electron-phonon interaction has a simple analytic representation in the two-dimensional pseudospin basis.³⁰ Using the results of Ref.30, the coupling matrix elements can be expressed in terms of the angles $\theta_{\mathbf{k}}$, $\theta_{\mathbf{q}}$ and $\theta_{\mathbf{k}+\mathbf{q}}$ of the involved wave vectors. Including contributions of order $O(q)$, we find that the coupling matrix elements in the long-wavelength limit takes the following form in the K -valley,

$$|M_{\mathbf{k}\mathbf{q}}^{TA}| = q\beta \times \left| \sin \left(2\theta_{\mathbf{q}} + \frac{\theta_{\mathbf{k}} + \theta_{\mathbf{k}+\mathbf{q}}}{2} \right) \right| \quad (6)$$

and

$$|M_{\mathbf{k}\mathbf{q}}^{LA}| = q \times \left| \alpha \cos \left(\frac{\theta_{\mathbf{k}+\mathbf{q}} - \theta_{\mathbf{k}}}{2} \right) + \beta \cos \left(2\theta_{\mathbf{q}} + \frac{\theta_{\mathbf{k}} + \theta_{\mathbf{k}+\mathbf{q}}}{2} \right) \right|, \quad (7)$$

for the TA and LA phonons, respectively. For the LA phonon, the first and second terms originate from

the deformation potential and the *gauge field* coupling mechanisms, respectively. The TA phonon couples only through the latter.^{30,38,39} Since the interaction is Coulombic in nature, the overall couplings given in Eqs. (6) and (7) are here referred to as deformation potential couplings.

With the coupling parameters listed in Table I, we find that the analytic expressions for the electron-phonon interaction in Eqs. (6) and (7) to a high degree reproduce the first-principles matrix elements for electron energies up to ~ 750 meV. As the analytic coupling matrix elements are based on the phonon modes in the long-wavelength limit, the agreement is slightly worsened at shorter wavelengths where the mode vectors deviate from the long-wavelength modes.³⁷ This is most pronounced for the TA phonon. As the LA phonon retains its long-wavelength character far out in the Brillouin zone, the agreement between the coupling matrix elements here remains quantitative even at shorter wavelengths. In the BG regime where short wavelength phonons are frozen out, we note that it is the long-wavelength limit of the coupling matrix elements that governs the scattering of carriers.

Often scattering on acoustic phonons is described by coupling to a single *effective* phonon mode with a coupling matrix element given by^{20,25}

$$M_{\mathbf{k}\mathbf{q}}^{\text{eff}} = \Xi_{\text{eff}} q \cos\left(\frac{\theta_{\mathbf{k},\mathbf{k}+\mathbf{q}}}{2}\right) \quad (8)$$

where Ξ_{eff} is the effective deformation potential and the angular part corresponds to the bare spinor overlap $\langle \chi_{\mathbf{k}+\mathbf{q}} | \chi_{\mathbf{k}} \rangle$ of the electronic wave function. In contrast to the more complex angular dependence of the coupling matrix element predicted by the full microscopic treatment presented here, the angular dependence of the *effective* coupling matrix element above suppresses only backscattering. In the high-temperature regime where equipartitioning of the acoustic phonons $N_{\mathbf{q}} \sim k_{\text{B}}T/\hbar\omega_{\mathbf{q}}$ applies, the relaxation time and the resistivity take the following simple forms²⁰

$$\frac{1}{\tau_{\mathbf{k}}} = \frac{1}{\hbar^3} \frac{\Xi_{\text{eff}}^2 k_{\text{B}} T}{4\rho v_{\text{F}}^2 c^2} \varepsilon_{\mathbf{k}} \quad ; \quad \rho = \frac{\pi \Xi_{\text{eff}}^2 k_{\text{B}} T}{4e^2 \hbar \rho v_{\text{F}}^2 c^2}, \quad (9)$$

where the factor of 4 in the denominators stems from the chiral nature of the carriers through the assumed form of the coupling matrix element in Eq. (8). These expressions are used almost exclusively to extract the value of the *effective* acoustic deformation potential in experimental situations.^{5,7-9,11}

IV. RESULTS

In the following, we study the intrinsic acoustic phonon-limited mobility of graphene in both the BG and linear resistivity regime using the full coupling matrix elements as given by Eqs. (6) and (7). This allows us

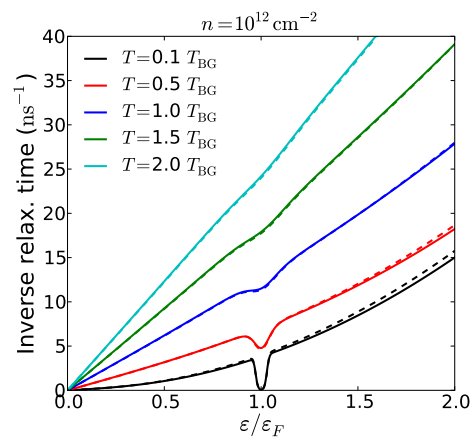


FIG. 2: (Color online) Inverse relaxation time (valley-averaged) for acoustic phonon scattering on the TA and LA phonon in the BG regime at $n = 10^{12} \text{ cm}^{-2}$ ($T_{\text{BG}} \approx 57 \text{ K}$). The full lines show the results obtained with the full matrix elements given in Eqs. (6) and (7) and coupling constants extracted from *ab-initio* calculations. The dashed lines show the result obtained with scattering on a single effective acoustic phonon with the coupling matrix element given by Eq. (8), a deformation potential of $\Xi_{\text{eff}} = 6.8 \text{ eV}$ and sound velocity $c = 20 \times 10^3 \text{ m/s}$.

to establish the value of the intrinsic *effective* acoustic deformation potential in graphene.

In Fig. 2 we show the inverse of the valley-averaged relaxation time as a function of energy for different temperatures and a carrier density of $n = 10^{12} \text{ cm}^{-2}$ corresponding to $\varepsilon_{\text{F}} \sim 117 \text{ meV}$ and $T_{\text{BG}} \approx 57 \text{ K}$ for the LA phonon. Above the BG temperature, the inverse relaxation time has the linear energy dependence of Eq. (9) and a slope proportional to the temperature. As the temperature is decreased below T_{BG} , the freezing out of short wavelength phonons and the sharpening of the Fermi surface result in limited phase space for phonon scattering and an increased life time of the carriers at the Fermi energy. In the expression for the relaxation time in Eq. (3) this effect is accounted for by the Fermi and Bose distribution functions. The limited phase space available for phonon scattering, manifests itself in the characteristic dip at the Fermi energy that evolves in the inverse relaxation time with decreasing temperature.²⁰ For all temperatures, the linear energy dependence of the high-temperature result in Eq. (9) is recovered in the $\varepsilon \rightarrow 0$ limit.

By inspecting the individual contributions, we find that the inverse relaxation time to a large extent is dominated by the contribution from the TA phonon both in the high-temperature and the BG regime. The domination of the TA phonon can be attributed to a number of factors. From Eq. (9) it follows directly that the lower sound velocity of the TA phonon leads to higher scattering rate. Also related to the sound velocity is the lower BG temperature of TA phonon which allows

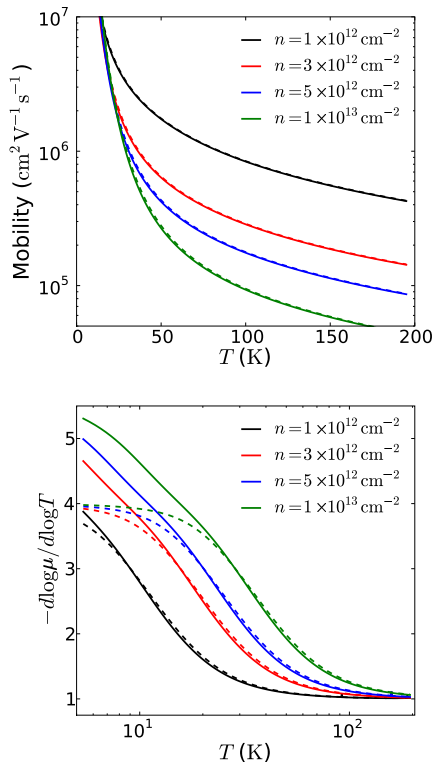


FIG. 3: (Color online) Mobility vs temperature for carrier densities $10^{12} - 10^{13} \text{ cm}^{-2}$ (upper plot). The lower plot shows the temperature dependence of the exponent α in the temperature dependence $\mu \sim T^{-\alpha}$ of the mobility.

for full backscattering below the BG temperature of the LA phonon. Secondly, the coupling matrix element for the TA phonon allows for backscattering which is suppressed for the LA phonon. In the BG regime, the domination of the TA phonon stems from the suppression of the coupling matrix element for the LA phonon in the long-wavelength limit (see Fig. 1). The observed dominance of the TA phonon is in contrast to the often used assumption that only the LA phonon couples to charge carriers in graphene.²⁰

In order to determine the intrinsic value of the *effective* deformation potential in graphene, we also calculate the relaxation time using coupling matrix element in Eq. (8). The dashed lines in Fig. 2 show the inverse relaxation time calculated with an *effective* deformation potential and sound velocity of 6.8 eV and $20.0 \times 10^3 \text{ m/s}$, respectively. It is seen to reproduce the relaxation time based on the full matrix elements very well for the energy range shown. While the extracted value for the acoustic deformation potential is much smaller than experimental values,^{5,7-9,11} it is in better agreement with recently reported *ab-initio* results yielding 4.5 eV.²³

Figure 3 summarizes the calculated acoustic phonon-limited mobility as a function of temperature for carrier densities $10^{12} - 10^{13} \text{ cm}^{-2}$. The mobility calculated with the above-mentioned *effective* coupling parameters

(dashed lines) reproduces the full calculation extremely well. For all carrier densities the mobility shows a transition from the linear $\mu \sim T^{-1}$ high-temperature behavior to a more pronounced $\mu \sim T^{-\alpha}$ temperature dependence with $\alpha > 1$ in the BG regime. At temperatures $T > T_{\text{BG}}$, the decrease in the mobility with increasing carrier density stems from the linear energy dependence of the density of states which provides more phase space for phonon scattering for higher Fermi levels. At low temperatures $T < T_{\text{BG}}$ where scattering on the full Fermi surface is frozen out, the local value of the coupling matrix element becomes important and the mobilities for the different carrier densities approach a common value.

The right plot shows the temperature dependence of the exponent α for the same set of carrier densities which correspond to BG temperatures $T_{\text{BG}} \sim 57 - 180 \text{ K}$ for the LA phonon. From this plot it is more clear that the departure away from the linear temperature dependence happens for $T \sim T_{\text{BG}}$. For $T < T_{\text{BG}}$, the exponent increases monotonically. Surprisingly, the exponents obtained from the mobility calculated with the full coupling matrix elements do not saturate at $\alpha = 4$ as predicted by the *effective* coupling matrix element (dashed lines).^{20,21} Thus, even in the absence of screening, the mobility of graphene should take on a temperature dependence with $\alpha > 4$ at sufficiently low temperatures. With carrier screening taken into account, this behavior is reinforced²¹

The purely intrinsic mobilities calculated here are significantly higher than previously reported theoretical values.²⁰ This is reflected directly in the extracted deformation potential parameter which is considerably lower than commonly used values. For a carrier density of $n = 10^{12} \text{ cm}^{-2}$ a room-temperature mobility in excess of $10^5 \text{ cm}^2 \text{ V}^{-1} \text{ s}^{-1}$ is here predicted. The associated scattering rate which is given by the relaxation time in Eq. (9) in the high-temperature regime, is from Fig. 2 estimated to be $\tau^{-1} \sim 10^{11} \text{ s}^{-1}$ at the Fermi level corresponding to a mean-free path of $\lambda = v_F/\tau \sim 1000 \text{ nm}$. Such an extremely large mean-free path may open the opportunity to study coherent transport in relatively large graphene structures. We note that the quasiparticle scattering rate observable in photoemission spectroscopy (ARPES) develops a similar dip at the Fermi level for $T < T_{\text{BG}}$ resulting in long-lived quasiparticles.

V. CONCLUSIONS AND DISCUSSIONS

In the present study the acoustic electron-phonon interaction in graphene has been analyzed in detail. The exact analytic forms of the coupling matrix elements in long-wavelength limit were found match the calculated first-principles matrix elements almost quantitatively even at shorter wavelengths. As previously predicted,^{20,21} the calculated mobilities showed a transition from a $\mu \sim T^{-1}$ to a $\mu \sim T^{-\alpha}$ temperature dependence with $\alpha > 1$ below the BG temperature. However, contrary to earlier studies we found that the full coupling

matrix elements cause the temperature dependence of the mobility to increase beyond $\alpha = 4$ which is otherwise only observed when screening is included.²¹

By fitting the results with an *effective* acoustic phonon the acoustic deformation potential is found to be $\Xi_{\text{eff}} = 6.8$ eV. Since this is much lower than the experimentally determined values 18 – 29 eV, our results suggest that the acoustic phonon-limited transport in substrate-supported graphene is at present not fully understood. Possible explanations for the large experimental deformation potentials could be (i) substrate-induced modifications of the band structure^{40,41} that modifies the chirality (and thereby the angular dependence of the coupling matrix element) of the electronic states and/or the Fermi velocity, and (ii) the existence of additional acoustic phonons not considered in the present work. This could be either the intrinsic flexural phonon which may be modified when graphene is lying on a substrate or surface-acoustic phonons on the substrate which have previously

been studied in 2DEGs.⁴² The relatively large variations in the experimental deformation potentials also indicate that the deformation potential depends on experimental factors such as e.g. the substrate.

Acknowledgments

The authors would like to thank T. Markussen and A.-P. Jauho for useful comments on the manuscript. KK has been partially supported by the Center on Nanostructuring for Efficient Energy Conversion (CNEEC) at Stanford University, an Energy Frontier Research Center funded by the U.S. Department of Energy, Office of Science, Office of Basic Energy Sciences under Award Number de-sc0001060. CAMD is supported by the Lundbeck Foundation.

-
- * Electronic address: cosby@fys.ku.dk
- ¹ K. S. Novoselov, A. K. Geim, S. V. Morozov, D. Jiang, Y. Zhang, S. V. Dubonos, I. V. Grigorieva, and A. A. Firsov, *Science* **306**, 666 (2004).
 - ² A. K. Geim and K. S. Novoselov, *Nature Mat.* **6**, 183 (2007).
 - ³ A. H. C. Neto, F. Guinea, N. M. R. Peres, K. S. Novoselov, and A. K. Geim, *Rev. Mod. Phys.* **81**, 109 (2009).
 - ⁴ S. Das Sarma, S. Adam, E. H. Hwang, and E. Rossi, *Rev. Mod. Phys.* **83**, 407 (2011).
 - ⁵ J.-H. Chen, C. Jang, S. Xiao, M. Ishigami, and M. S. Fuhrer, *Nature Nano.* **3**, 206 (2008).
 - ⁶ E. H. Hwang and S. Das Sarma, *Phys. Rev. B* **79**, 165404 (2009).
 - ⁷ D. K. Efetov and P. Kim, *Phys. Rev. Lett.* **105**, 256805 (2010).
 - ⁸ C. R. Dean, A. F. Young, I. Meric, C. Lee, L. Wang, S. Sorgenfrei, K. Watanabe, T. Taniguchi, P. Kim, K. L. Shepard, et al., *Nature Nano.* **5**, 722 (2010).
 - ⁹ K. Zou, X. Hong, D. Keefer, and J. Zhu, *Phys. Rev. Lett.* **105**, 126601 (2010).
 - ¹⁰ A. Pachoud, M. Jaiswal, P. K. Ang, K. P. Loh, and B. Özyilmaz, *Europhys. Lett.* **92**, 27001 (2010).
 - ¹¹ K. I. Bolotin, K. J. Sikes, J. Hone, H. L. Stormer, and P. Kim, *Phys. Rev. Lett.* **101**, 096802 (2008).
 - ¹² J. Xue, J. Sanchez-Yamagishi, D. Bulmash, P. Jacquod, A. Deshpande, K. Watanabe, T. Taniguchi, P. Jarillo-Herrero, and B. J. LeRoy, *Nature Mat.* **10**, 282 (2011).
 - ¹³ R. Decker, Y. Wang, V. W. Brar, W. Regan, H.-Z. Tsai, Q. Wu, W. Gannett, A. Zettl, and M. F. Crommie, *Nano. Lett.* **11**, 2291 (2011).
 - ¹⁴ C. R. Dean, A. F. Young, P. Cadden-Zimansky, L. Wang, H. Ren, K. Watanabe, T. Taniguchi, P. Kim, J. Hone, and K. L. Shepard, *Nature Phys.* **7**, 693 (2011).
 - ¹⁵ P. J. Zomer, S. P. Dash, N. Tombros, and B. J. van Wees, *Appl. Phys. Lett.* **99**, 232104 (2011).
 - ¹⁶ S. Fratini and F. Guinea, *Phys. Rev. B* **77**, 195415 (2008).
 - ¹⁷ A. Konar, T. Fang, and D. Jena, *Phys. Rev. B* **82**, 115452 (2010).
 - ¹⁸ X. Li, E. A. Barry, J. M. Zavada, M. B. Nardelli, and K. W. Kim, *Appl. Phys. Lett.* **97**, 232105 (2010).
 - ¹⁹ J. M. Ziman, *Electrons and phonons* (Oxford University Press, London, 1960).
 - ²⁰ E. H. Hwang and S. Das Sarma, *Phys. Rev. B* **77**, 115449 (2008).
 - ²¹ H. Min, E. H. Hwang, and S. Das Sarma, *Phys. Rev. B* **83**, 161404 (2011).
 - ²² V. Perebeinos and P. Avouris, *Phys. Rev. B* **81**, 195442 (2010).
 - ²³ K. M. Borysenko, J. T. Mullen, E. A. Barry, S. Paul, Y. G. Semenov, J. M. Zavada, M. B. Nardelli, and K. W. Kim, *Phys. Rev. B* **81**, 121412 (2010).
 - ²⁴ R. S. Shishir and D. K. Ferry, *J. Phys.: Condens. Matter* **21**, 232204 (2009).
 - ²⁵ T. Stauber, N. M. R. Peres, and F. Guinea, *Phys. Rev. B* **76**, 205423 (2007).
 - ²⁶ L. M. Woods and G. D. Mahan, *Phys. Rev. B* **61**, 10651 (2000).
 - ²⁷ E. V. Castro, H. Ochoa, M. I. Katsnelson, R. V. Gorbachev, D. C. Elias, K. S. Novoselov, A. K. Geim, and F. Guinea, *Phys. Rev. Lett.* **105**, 266601 (2010).
 - ²⁸ K. Kaasbjerg, K. S. Thygesen, and K. W. Jacobsen, *Phys. Rev. B* (2012), submitted.
 - ²⁹ J. . Enkovaara, C. Rostgaard, J. J. Mortensen, J. Chen, M. Dulak, L. Ferrighi, J. Gavnholt, C. Glinsvad, V. Haikola, H. A. Hansen, et al., *J. Phys.: Condens. Matter* **22**, 253202 (2010).
 - ³⁰ J. L. Mañes, *Phys. Rev. B* **76**, 045430 (2007).
 - ³¹ E. H. Hwang, S. Adam, and S. Das Sarma, *Phys. Rev. Lett.* **98**, 186806 (2007).
 - ³² B. Wunsch, T. Stauber, F. Sols, and F. Guinea, *New J. Phys.* **8**, 318 (2006).
 - ³³ E. H. Hwang and S. Das Sarma, *Phys. Rev. B* **75**, 205418 (2007).
 - ³⁴ Since $c_{\lambda}/v_F \sim 10^{-2}$ for graphene, the acoustic phonon energy can to a good approximation be neglected in argument of energy conserving δ -functions of Eq. (4).

³⁵ For the numerical evaluation of Eq. (3), the identity

$$f_{\mathbf{k}}(1 - f_{\mathbf{k}\pm\mathbf{q}})N_{\pm\mathbf{q}} = f_{\mathbf{k}\pm\mathbf{q}}(1 - f_{\mathbf{k}})(1 + N_{\pm\mathbf{q}}),$$

where $f_{\mathbf{k}\pm\mathbf{q}} = f(\varepsilon_{\mathbf{k}} \pm \hbar\omega_{\mathbf{q}})$ and $N_{\pm\mathbf{q}} = N(\pm\hbar\omega_{\mathbf{q}})$ is understood, comes in very handy.

³⁶ The coupling matrix elements for the electron-phonon coupling have been calculated within DFT-LDA using a 7×7 supercell and a DZP basis for the electronic Bloch states.

³⁷ At shorter wavelengths, the strictly transverse and longitudinal character of the modes vanishes. For the TA phonon this implies that the transverse character is only retained in certain high symmetry directions of the Brillouin zone.

For the LA phonon we find that the mode vector retains its long-wavelength character for q -values up to $\sim 30\%$ of the Brillouin zone size.

³⁸ E. Mariani and F. von Oppen, Phys. Rev. Lett. **100**, 076801 (2008).

³⁹ E. Mariani and F. von Oppen, Phys. Rev. B **82**, 195403 (2010).

⁴⁰ C. Ortix, L. Yang, and J. van den Brink, arXiv:1111.0399v1 (2011).

⁴¹ C.-H. Park, L. Yang, Y.-W. Son, M. L. Cohen, and S. G. Louie, Phys. Rev. Lett. **101**, 126804 (2008).

⁴² A. Knäbchen, Phys. Rev. B **55**, 6701 (1997).